ELSEVIER

Polymer 43 (2002) 2295–2309

polymer

www.elsevier.com/locate/polymer

Gas transport behavior of semicrystalline syndiotactic polystyrene containing α and β crystalline forms

T. Prodpran, S. Shenogin, S. Nazarenko*

Department of Macromolecular Science and Center for Applied Polymer Research, Case Western Reserve University, Cleveland, OH 44106, USA

Received 21 September 2001; received in revised form 10 December 2001; accepted 12 December 2001

Abstract

Solid-state structure of syndiotactic polystyrene (s-PS) after crystallization from the melt and the glassy state was examined by differential scanning calorimetry, density and X-ray diffraction analysis (WAXS). It was possible to prepare semicrystalline s-PS containing pure α (α″ or α′ modifications) and pure β crystalline forms with different crystallinities (0–40%). The measurements confirmed the low density of both crystalline forms, which in the case of α crystalline form was smaller and in the case of β crystalline form was slightly larger than the density of the glassy amorphous s-PS. Oxygen and carbon dioxide gas permeability, diffusion and solubility of semicrystalline s-PS containing different crystalline forms were studied as a function of crystallinity. These measurements confirmed that more dense β crystalline form was impermeable for the transport of small gas molecules while less dense α crystalline form was highly gas permeable. Unusual gas transport behavior of the α crystalline form was attributed to porous crystalline structure containing the nanochannels. Despite the porous structure, α crystalline form showed very low oxygen and carbon dioxide solubility compared to gas solubility in the amorphous phase. The proposed diffusion model explained the characteristic features of the gas permeation behavior for chemically 'inert' small gas molecules in the permeation medium consisting of glassy amorphous polymer with dispersed porous crystalline phase containing the nanochannels. A new relaxation process with the maximum at about −35 °C was observed in semicrystalline s-PS containing the α crystals and was associated with the porous structure of this crystalline form. © 2002 Published by Elsevier Science Ltd.

Keywords: Syndiotactic polystyrene (s-PS); Gas Transport; Crystallinity

1. Introduction

Syndiotactic polystyrene shows a very complex polymorphic behavior. Four main polymorphic crystalline structures were assigned by Guerra et al., as α, β, γ, and δ [1]. These various crystalline forms differ by the conformation order and by the mode of crystalline packing of chains having the same conformation order. Two solvent-induced crystalline forms γ and δ contain helical chains with conformational order TTGG and identity period $c = 7.8$ Å. Thermal crystallization results in either α or β crystalline forms. Both α or β crystalline forms contain chains exhibiting planar zigzag conformation order (TTTT) with identity period $c = 5.1$ Å. Fig. 1(a)–(c) shows models of α and β crystalline forms drawn to scale. Carbon and hydrogen atoms are also drawn approximately according to their van der Waals radii.

The structure of the β crystalline form (Fig. 1(a)), first proposed by Chatani et al., is usual [2]. This crystalline form is characterized by orthorhombic chain packing with unit cell dimensions $a = 8.81$ Å, $b = 28.82$ Å, and $c = 5.1$Å. The crystalline density of the β crystalline form, 1.068 g/cm^3, was calculated from the parameters of the unit cell and it is slightly larger than the density of the amorphous s-PS [3].

The α form is unusual, and its crystalline structure has no known analogue among the synthetic polymers. Two different modifications of the α form having different degrees of structural order have to be mentioned here. The α structure obtained upon cold crystallization from the glassy state is known as limiting disordered modification α′, while the α form obtained upon crystallization from the melt state is known as limiting ordered modification α″ [4]. The chains in the α crystalline form are first packed in clusters (triplets) each containing three chains. The backbones of these three chains make a core of the triplet while the phenyl rings are pointed toward the periphery. The triplets form a 'superstructure'. The relative arrangement of triplets in the superstructure still remains a subject of the controversy despite the numerous efforts to resolve this puzzle. In the model of the α″ structure proposed by

* Corresponding author.
E-mail address: sin@po.cwru.edu (S. Nazarenko).

0032-3861/02/$ - see front matter © 2002 Published by Elsevier Science Ltd.
PII: S0032-3861(02)00026-5

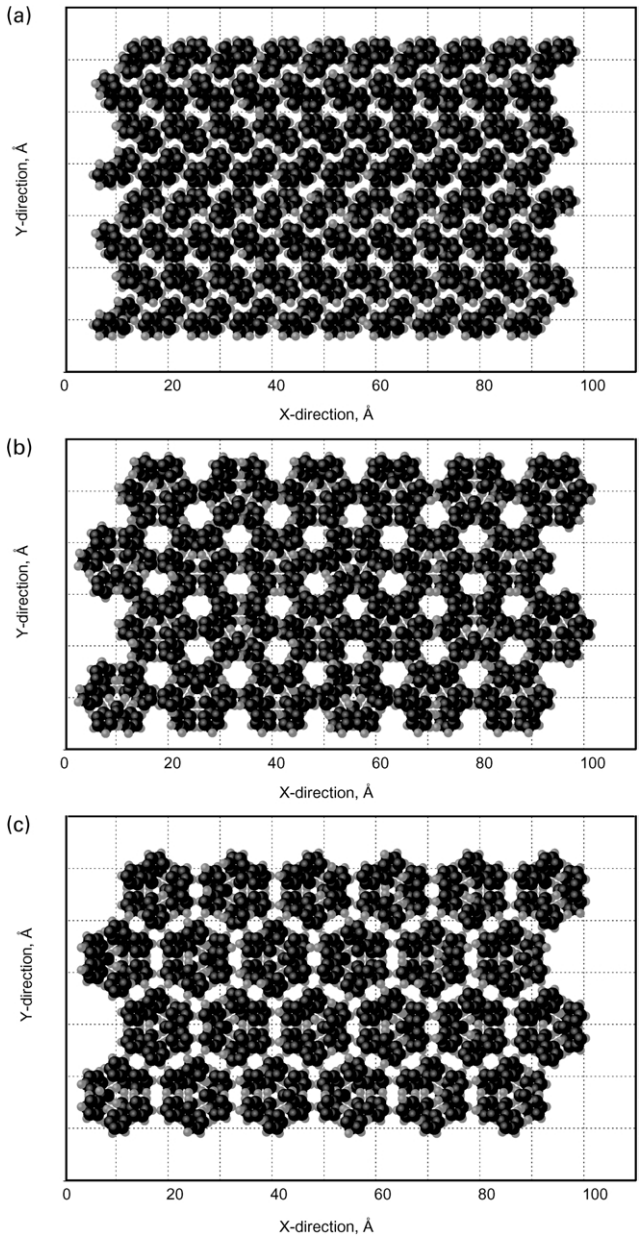

Fig. 1. Scale models of β and α crystalline forms of s-PS: (a) β crystalline form; (b) α crystalline form (Greis); (c) α crystalline form (De Rosa).

Greis (Fig. 1(b)) three triplets are included in a trigonal unit cell with unit cell dimensions $a = b = 26.26$ Å, $c = 5.1$ Å [5]. The triplets are also considered at the same height with two identically positioned triplets and one rotated by 180°. Greis also proposed a one-triplet trigonal model for the α' structure. In his first model of the α'' structure, De Rosa proposed that the triplets have a relative shift $c/3$ along c axis and rotated by 30° relative to azimuthal position of the triplets in the Greis model (Fig. 1(c)) [4]. In the last modification of the model, the triplets are rotated by an additional angle 7° [6]. Limiting ordered modification, α'', according to De Rosa, shows an order in the positioning of the triplets, e.g. considering any three adjacent triplets in the structure, one triplet is always oriented in one direction and the other two are rotated by 60° relative to the orientation of the first triplet. Although the orientation of one and the other two triplets are different, these two orientations are isosteric with respect to the orientation of the phenyl rings. The phenyl rings in each triplet are oriented in the same manner despite the triplet rotation. In the limiting disordered modification, α', the distribution of the two isosteric orientations between triplets is random.

Recently, Lotz et al. suggested an alternative model of the frustrated crystalline structure of the α form in which the azimuthal orientations of the three triplets is different from those considered by Greis and De Rosa [7]. In this model, the azimuthal settings and relative shifts of the triplets are such that two triplets maximize their interactions, while the third interacts less favorably with its neighbors. This model showed so far the best agreement with the experimental electron diffraction pattern of the corresponding single crystal of the α form.

The inability of X-ray, in comparison with other techniques, to detect large amount of crystalline phase in s-PS, especially when it was formed upon annealing at relatively low temperatures above T_g was recognized earlier and related to the formation of the mesomorphic phase associated with the conformational order inside the chains (plane chain zigzag) and with paracrystalline disorder between the chains [8]. More recently, the detailed structural analysis of mesomorphic structure was conducted by Auriemma et al. using X-ray diffraction and FTIR [9]. They concluded that the mesomorphic phase consists of triplets of polystyrene chains, rather than randomly spaced chains with conformational order as it was originally thought, with complete order inside the triplets and paracrystalline disorder between the triplets.

Despite the differences, all models of the α crystalline form predict the same density, 1.033 g/cm^3, which is smaller than the density of the amorphous phase. However, the models predict different distribution of an unoccupied space in crystalline s-PS, which is responsible for the low density of α crystals. In the Greis model, the structure exhibits wide opened channels. Six channels, adjacent to the sides of each triplet, have almost circular aperture about 5 Å in diameter. In the De Rosa model of the α form, the unoccupied space almost uniformly surrounds each triplet in the form of hollow hexagonal prism with the thickness about 3–4 Å. In the model proposed by Lotz, the distribution of an unoccupied space is more complex and resembles some features existing in both Greis and De Rosa models. The low-density crystalline structure of the α form raises several interesting questions such as whether this crystalline structure is permeable for transport of small gas molecules, what is the contribution of crystalline and amorphous phases to the entire diffusion mechanism in the semicrystalline polymer, what is the role of crystalline morphology. Typically, the density of polymer crystals is larger than the density of amorphous phase by 10–15%, and polymer crystals are considered

practically impermeable for transport of small gas molecules. Recently, we showed that both α'' and α' modifications of the α form were permeable to small gas molecules such as oxygen and carbon dioxide [10]. This behavior was very unusual and has been previously reported only for one other synthetic polymer, isotactic poly(4-methyl-pentene1) (P4MP1), which in fact also demonstrates the low density of the crystalline structure [11]. The uniformity of relatively large inter-chain gaps in low-density crystals of s-PS as well as P4MP1 makes the polymers of this kind, potentially very interesting materials for molecular sieving applications. In turn, the β crystalline form of s-PS was found to be practically impermeable to oxygen and carbon dioxide [10]. Despite that these important conclusions about the gas transport properties of thermally induced crystalline forms of s-PS have been made, the analysis considered in our first report was limited by the fact that we could not vary the crystallinity and control the crystalline morphology. All semicrystalline samples were obtained during non-isothermal cooling in the press after compression molding. Therefore, neither crystallinity nor crystalline morphology of the pure α'' and β form was feasible to control under these conditions. Most of the samples studied earlier, containing the limiting disordered modification α' also contained the β crystalline form. This made it virtually impossible to compare the gas transport properties of two modifications of the α form.

Therefore, the overall goal of this study was to expand our previous work [10]. We planned to prepare semicrystalline s-PS containing pure β as well as two pure modifications (α'' and α') of the α crystalline form with different crystallinity and controlled morphology, and then to study and compare oxygen and carbon dioxide gas transport behavior of these polymers and some other related properties.

2. Experimental

Syndiotactic polystyrene with average molecular weight $M_w \approx 300\,000$ g/mol and polydispersity $M_w/M_n \approx 2$ was supplied by the Dow Chemical Company, Midland, MI in the pellet form.

2.1. Preparation of the α'' crystalline form

Samples containing pure α'' crystalline form with various degrees of crystallinity were prepared using isothermal crystallization from the melt. First, specimens in the form of 165 mm × 165 mm wide and 400 μm thick rectangular plaques were prepared by compression molding of melted pellets directly between two polished steel platens. The pellets were placed in the press and preheated at mold temperature 280 °C for 45 min without pressure. Then, the pressure was increased to 30 000 psi and released; this cycle was repeated two times to ensure that the plaques would be free of bubbles. Finally, the platens were held at 30 000 psi for 5 min and the pressure finally released. Then, the platens with the sample between were rapidly transferred to the convection oven which was preset at crystallization temperature $T_c = 260$ °C. In the oven, the samples were isothermally crystallized for different times. After the crystallization was completed, the samples were rapidly quenched into ice–water mixture and then dried under vacuum.

2.2. Preparation of the α' crystalline form

Samples containing the α' crystalline form were prepared via cold crystallization. First, the amorphous samples were prepared. To prepare the amorphous samples, plaques were molded at 315 °C for 15 min and then quenched into ice–water mixture. Amorphous samples were sandwiched between the steel platens, placed to the oven and annealed using the following procedure. The temperature of the oven was slowly increased at about 5 °C/min from room temperature to the final crystallization temperature ranging from 100 to 260 °C. The samples were kept at the final crystallization temperature for 30 min. After cold-crystallization, the samples were quenched into cold water and dried under vacuum.

2.3. Preparation of the β crystalline form

The β crystalline form was prepared in a manner similar to the preparation of the α'' form. However, the compression molding temperature was 330 °C, preheating time was 10 min, and the oven for isothermal crystallization was preset at 250 °C. To vary the crystallinity, samples were isothermally crystallized at different times in the oven and then quenched to ice–water mixture.

2.4. Measurements

The crystalline structure was studied using wide-angle X-ray scattering measurements conducted with automatic powder diffractometer Phillips Model APD 3520 using nickel filtered Cu Kα radiation (wavelength 1.542 Å). Powder samples were scanned within scattering angle range 2θ from 5 to 30° at 0.001 °/min. The X-ray degree of crystallinity was calculated from the intensities scattered by the crystalline and amorphous regions. The experimental peak intensities were corrected using Lorentz factor $L = 1/(\sin^2\theta \cos\theta)$.

The differential scanning calorimetry (DSC) experiments were carried out using Rheometrics Scientific DSC Plus. The instrument was calibrated with indium, tin, lead and sapphire standards. Heating scans were recorded at 10 °C/min.

The dynamic mechanical measurements were conducted using Rheometrics Scientific DMTA V™ instrument at frequency 1 Hz.

Density was measured using gradient column constructed from liquid solution of diethylene glycol/isopropanol in accordance with ASTM-D 1505 Method B. The column

was calibrated with glass floats of known density. Small pieces (~25 mm^2) were placed in the column and allowed to equilibrate before the measurements were taken. The experimental error of the density measurements did not exceed ± 0.0005 g/cm^3. The volume crystalline fraction from density was calculated using a simple two-phase model assuming constant density of amorphous and crystalline phases $\phi_c = (\rho - \rho_a)/(\rho_c - \rho_a)$, where ρ, ρ_c and ρ_a are the densities of the sample, pure crystalline and pure amorphous phases, respectively.

Oxygen and carbon dioxide flux $J(t)$ (testing area 50 cm^2) at 25 °C, 0% relative humidity, and 1 atm pressure was measured with MOCON OX-TRAN® and MOCON PERMATRAN®-C/440. Both instruments use a continuous-flow cell method that is approved by ASTM (Designation: D 3985-81) and are designed for measurements of oxygen and carbon dioxide permeation through polymers. Nitrogen was the carrier gas and either 100% oxygen or 100% carbon dioxide was the test gas. The details of the measurement technique adopted in our lab are described elsewhere [12]. Permeability P and diffusion coefficient D were obtained by performing a two parametric least square fit of the experimental permeation flux data to the solution of Fick's second law

$$J(t) = \frac{Pp}{l}\left(1 + 2\sum_{n=1}^{\infty}(-1)^n \exp(-D\pi^2 n^2 t/l^2)\right), \quad (1)$$

where $J(t)$ is the flux, P, the permeability coefficient, D, the diffusion coefficient, l, the bulk sample thickness and p is the gas pressure. The solubility S was obtained from the relationship $P = DS$. The bulk thickness l for each specimen was determined after the barrier measurement was completed. A $3 \times 3''$ square section was cut from the tested area. The weight W and area A of the cut sample were accurately measured. The bulk thickness was calculated as $l = W/A\rho$, where ρ is the measured density.

3. Results and discussion

3.1. Solid state structure

The crystallographic structure of α and β crystalline forms of s-PS has been intensively studied for the last 10 years primarily using WAXS [1,–7,13,14]. The proposed crystallographic models are described in Section 1. This section aims primarily to present the WAXS data confirming that the proposed in this work crystallization conditions indeed resulted in the formation of pure α'', α' and β' crystalline forms, based on the WAXS peak assignments made previously.

Fig. 2(a) shows WAXS diffractograms of samples, compression molded at 280 °C and melt crystallized at 260 °C for various times. The corresponding maximums were located at $2\theta = 6.7$(110), 10.3 (210), 11.7 (300), 13.5 (220), 14.0 (310), 15.6 (400), 17.9 (410), 20.4 (211), 22.2 (510) and 23.8° (600). Fig. 2(b) shows WAXS diffractograms of s-PS cold crystallized for 30 min at various temperatures. Samples annealed at 120 °C exhibited the diffraction pattern, which was practically indistinguishable from the amorphous halo. Annealing at 130 °C, a temperature within the cold crystallization range of s-PS, resulted in some distinguishable changes in the form of X-ray diffractogram compared to that for amorphous sample. The diffractogram revealed practically the same two-peak feature typical of the amorphous halo. However, the peak maximums shifted toward the larger scattering angles and the main amorphous halo peak significantly sharpened. Annealing in the range 140–260 °C showed the appearance and sharpening of three broad reflections located at $2\theta = 6.7°$(110), 11.7° (300) and 13.5° (220). Starting at 230 °C, the reflection at $2\theta = 17.9°$(410) and 23.8° (600) also became apparent.

Maximums located at $2\theta = 6.7$, 11.7, 13.5, 17.9, 20.4, 22.2 and 23.8° are generally assigned to the α crystalline form in the case of crystalline s-PS [4–6]. Three additional characteristic peaks in the diffractograms, shown in Fig. 2(a), located at $2\theta = 10.3$, 14 and 15.6° are specific for limiting ordered modification α'' of the α form. These three peaks are absent in the case of limiting disordered modification, α', of the α form obtained upon cold crystallization (Fig. 2(b)). Fig. 2(c) shows WAXS diffractograms of samples compression molded at 330 °C and melt crystallized for various times at 250 °C. All samples revealed the diffraction pattern, typical of pure β crystalline form. The diffractograms contained characteristic peaks, at $2\theta = 6.2$ (020), 10.4 (110), 12.2 (040), 13.6 (130), 18.6 (060), 20.2 (111), 21.3 (041), 23.9 (170) and 24.9° (080), which are generally attributed to the β form [1,3,13,14].

3.2. Measurements of crystallinity

Reliable and accurate measurement of crystallinity is an important step in order to relate the crystallinity to gas transport behavior in semicrystalline polymers. In our first attempt [10], we mainly used DSC and X-ray (WAXS) methods to determine the crystallinine fraction in semicrystalline s-PS. Both methods showed some limitations, especially if samples were cold crystallized. For cold-crystallized s-PS, we showed that DSC method overestimates the amount of crystallinity because it measures the total amount of ordered phase, which, in fact, represents the sum of the mesomorphic and the crystalline phases. Although X-ray methods measure the amount of crystalline phase only, this method is cumbersome and sensitive to the procedure by which the amorphous contribution to the overall diffraction scattering is subtracted. In this work, we tried to explore the density method to determine the crystallinity for both melt and cold-crystallized s-PS.

The density method requires knowing the density of pure amorphous and pure crystalline s-PS. The densities of pure crystalline s-PS in the case of either α and β forms can be

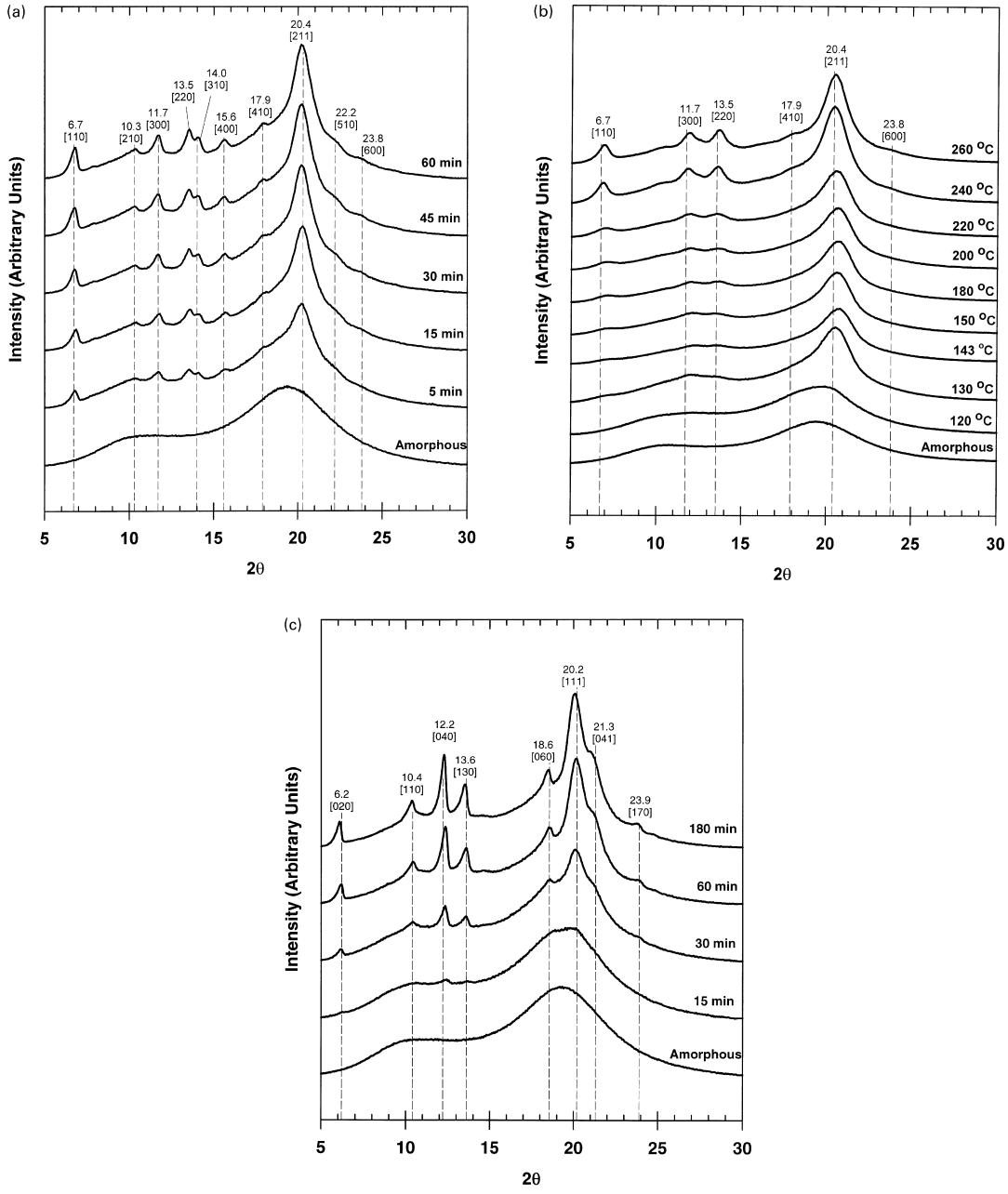

Fig. 2. WAXS diffractograms of amorphous and semicrystalline s-PS: (a) molded at 280 °C and isothermally melt-crystallized at 260 °C for various times; (b) cold crystallized from amorphous glassy state for 30 min at various temperatures; (c) molded at 330 °C and isothermally crystallized at 250 °C.

determined very accurately based on the unit cell dimensions of these crystalline forms. The corresponding densities are 1.033 and 1.068 g/cm^3, respectively. The amorphous density has to be experimentally measured. The measurements of amorphous density were undertaken on a series of thin, about 100 μm, s-PS samples quenched after compression molding into ice–water mixture. The amorphous density was found to be 1.0490 ± 0.0005 g/cm^3. In our previous study, we also measured the density of quenched s-PS, and it showed a smaller value. However, the samples which we studied previously were too thick (1 mm), and capable of developing some crystallinity even on quenching into ice–water mixture.

Fig. 3 shows the dependence of density for melt-crystallized s-PS versus time. As expected, the density decreased and then leveled off with time in the case when low-density α crystalline structure was formed, and increased and then leveled off with time when more dense β crystalline structure was formed. Fig. 4 shows the plot of density versus annealing temperature for cold-crystallized samples. Starting at 120 °C, the density progressively decreased with temperature, which is associated with more

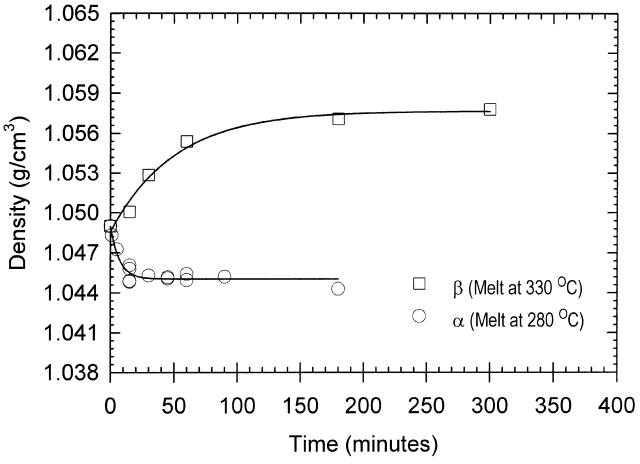

Fig. 3. Density changes versus crystallization time for melt-crystallized s-PS containing α'' and β crystalline forms.

pronounced at elevated annealing temperatures formation of low-density α crystalline structure.

Accurate measurements of DSC crystallinity depend on knowing the correct value of heat of fusion for one hundred percent crystalline polymer. For s-PS, the value 53.2 J/g is generally used. This value was obtained by Passztor et al. [15] using extrapolation of the change in specific heat capacity at glass transition plotted versus $\Delta H = H_m - H_{cc}$ toward zero change for a series of differently crystallized s-PS, where H_m is the enthalpy of melting and H_{cc} is the enthalpy of cold crystallization. The heat of fusion for one hundred percent crystalline polymer, in fact, can also be determined from the density and DSC data. Fig. 5 shows the plot of $\Delta H = H_m - H_{cc}$ versus density for melt-crystallized samples containing pure α and β crystalline structures. The linear regression extrapolated toward the density of pure α and β form showed that despite a significant structural difference between the two crystalline forms, the values of heat of fusion for one hundred percent crystalline polymer for both forms are surprisingly similar, 50 ± 1

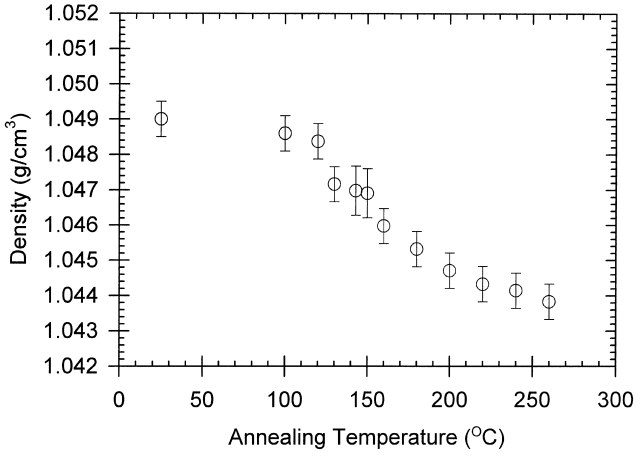

Fig. 4. Density changes versus annealing temperature for cold-crystallized s-PS containing α' crystalline form.

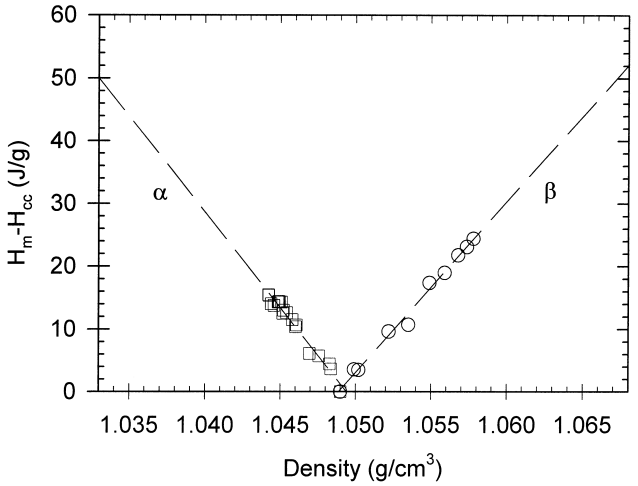

Fig. 5. Heat of fusion, $\Delta H = H_m - H_{cc}$, versus density for melt-crystallized s-PS containing α'' and β crystalline forms.

and 52 ± 1 J/g, respectively, and exhibit an excellent agreement with the value reported by Pasztor et al.

The amount of crystallinity determined by density, DSC and X-ray method for melt-crystallized samples are shown in Table 1. For the heat of fusion of one hundred percent crystalline polymer, we used the values obtained in the present work. For melt-crystallized samples containing the α form, we found an excellent agreement between DSC, X-ray and density methods. For the β form, although there was an excellent agreement between DSC and density crystallinity, X-ray persistently showed slightly smaller values. The origin of this discrepancy is currently unclear. Table 1 also reports DSC, X-ray and density crystallinities for cold-crystallized samples. While at low annealing temperatures the DSC crystallinity was significantly larger than the X-ray crystallinity, the difference practically disappeared at high annealing temperatures. The difference between DSC and X-ray crystallinity decreased due to the conversion of the mesomorphic phase into well formed α crystals at elevated annealing temperatures. The density also decreased with increase in annealing temperature. One can also see that despite the significant amount of ordered phase developed at low annealing temperatures (DSC crystallinity), the density changes are very insignificant. For instance, after annealing at 120 °C, which earlier was associated with the formation of the mesomorphic phase only [9], despite that DSC showed 22% of ordered phase, the density changes were within the experimental scatter.

Based on this observation, one may conclude that the density of the mesomorphic phase is very similar to that for pure amorphous phase. Hence, despite that cold-crystallized samples contained amorphous phase, mesomorphic phase and crystalline phase, the crystalline fraction can be calculated based on two-phase model assuming equal densities for amorphous and mesomorphic phases. The density crystallinities for cold-crystallized samples are

Table 1
Densities and crystallinities of isothermally melt-crystallized and cold-crystallized s-PS

Materials	Density (g/cm^3)	Density crystallinity	DSC crystallinity	X-ray crystallinity
Amorphous-PS	1.0490 ± 0.0005	0	0	0
s-PS Melt (280 °C) crystallized (α'') for				
5 min	1.0473 ± 0.0005	0.11 ± 0.02	0.11 ± 0.01	0.09 ± 0.01
15 min	1.0454 ± 0.0005	0.22 ± 0.02	0.24 ± 0.02	0.17 ± 0.04
30 min	1.0453 ± 0.0005	0.23 ± 0.03	0.23 ± 0.03	0.23 ± 0.03
45 min	1.0451 ± 0.0005	0.24 ± 0.03	0.25 ± 0.03	0.26 ± 0.04
60 min	1.0452 ± 0.0005	0.24 ± 0.03	0.25 ± 0.03	0.27 ± 0.04
90 min	1.0452 ± 0.0005	0.24 ± 0.03	0.24 ± 0.03	0.26 ± 0.04
180 min	1.0443 ± 0.0005	0.29 ± 0.03	0.28 ± 0.03	0.24 ± 0.03
s-PS Melt (330 °C) crystallized (β) for				
15 min	1.0501 ± 0.0005	0.06 ± 0.01	0.07 ± 0.01	0.02 ± 0.02
30 min	1.0529 ± 0.0005	0.20 ± 0.02	0.19 ± 0.02	0.12 ± 0.02
60 min	1.0554 ± 0.0005	0.34 ± 0.04	0.34 ± 0.03	0.27 ± 0.04
180 min	1.0571 ± 0.0005	0.43 ± 0.05	0.42 ± 0.04	0.29 ± 0.06
s-PS Cold-crystallized (α') at				
120 °C	1.0484 ± 0.0005	0.04 ± 0.01	0.22 ± 0.02	0.02 ± 0.02
130 °C	1.0472 ± 0.0005	0.12 ± 0.01	0.48 ± 0.05	0.17 ± 0.03
160 °C	1.0460 ± 0.0005	0.19 ± 0.02	0.47 ± 0.05	0.22 ± 0.03
180 °C	1.0453 ± 0.0005	0.23 ± 0.03	0.46 ± 0.05	0.26 ± 0.04
200 °C	1.0447 ± 0.0005	0.27 ± 0.03	0.45 ± 0.04	0.26 ± 0.04
220 °C	1.0443 ± 0.0005	0.29 ± 0.03	0.45 ± 0.04	0.28 ± 0.04
240 °C	1.0441 ± 0.0005	0.30 ± 0.04	0.46 ± 0.05	0.33 ± 0.05

reported in Table 1. We found a very good agreement between the density crystallinities and X-ray crystallinities for all cold-crystallized s-PS. It is an interesting question why the density of the mesomorphic phase and the density of isotropic, amorphous phase are similar in s-PS. Taking into account that the mesomorphic phase in s-PS, as it is defined [8], resembled certain features of nematic liquid crystalline order, it was also interesting to explore whether the transition from isotropic, amorphous state to nematic liquid crystalline state was also associated with much smaller density changes compared to that from isotropic to normal crystalline state. Indeed, the density changes associated with the transition from isotropic to nematic liquid crystalline order in general are very small as compared with the density changes associated with the transition from isotropic to crystalline state [16]. This fact, most likely, is associated with much weaker inter-chain interaction responsible for the nematic liquid crystalline order in comparison with inter-chain interaction responsible for crystalline order.

3.3. Gas permeation behavior

Fig. 6(a) and (b) shows several examples of experimental oxygen flux curves (experimental points), $J(t)$, measured at room temperature for amorphous and s-PS containing different amounts of the β crystalline phase (Fig. 6(a)) and s-PS containing different amount of the α'' phase. All curves consisted of a non-steady and a steady state region. The non-steady state region, associated with the progress of concentration profile across the thickness, is mainly determined by the diffusion coefficient D. As the permeant concentration in the specimen reached a constant distribution, the flux reached the steady-state value, J_0. This value normalized by film thickness l and permeant pressure p defined the permeability $P = J_0 l p^{-1}$. In the first approximation, P and D can be roughly estimated from two characteristic features of the flux curves. P is directly proportional to the steady state flux value, J_0, and D is reciprocally proportional to the time, $\tau_{1/2}$, for the flux to reach one half of its steady state value [17]. The half-time for each permeation curve is indicated in the Fig. 6(a) and (b).

Oxygen steady state flux decreased for semicrystalline s-PS, containing the β crystalline form (Fig. 6(a)) in comparison with that for amorphous s-PS, the non-steady state region, however, practically did not change indicating the constancy of the diffusion coefficient. Oxygen steady state flux significantly increased (larger permeability) and non-steady region significantly shortened (faster diffusion) with the crystallinity for semicrystalline s-PS containing the α'' crystalline form (Fig. 6(b)).

Accurate values of permeability P, and diffusion coefficient D, were obtained by performing a two parametric least square fit of the experimental flux data to Eq. (1). The fitting curves are included with the experimental points in Fig. 6(a) and (b). The fits were equally good for all the experiments in this study. The error in determining the two fitting parameters Pl^{-1} and Dl^{-2}, was estimated not to exceed 4%.

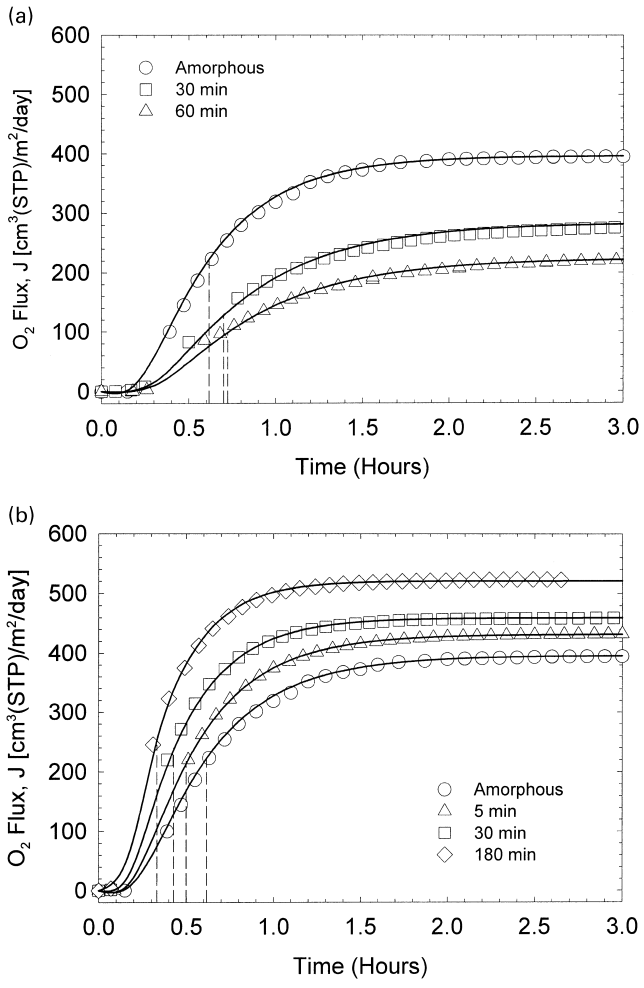

Fig. 6. Experimental oxygen flux versus time data and the fit to Fick's law for amorphous and semicrystalline s-PS: (a) containing different amount of the β phase after isothermal crystallization for various times; (b) containing different amount of the α'' phase after isothermal crystallization for various times.

Thus the main sources of error in calculating P and D was determined mainly by the accuracy of the bulk average thickness measurements. For this reason, special attention was paid to the bulk average thickness measurement as described in Section 2.

3.3.1. Analysis of the β crystalline form

Fig. 7(a)–(c) shows oxygen permeability, diffusion and solubility for the β crystalline form plotted as a function of crystalline fraction. The amount of crystalline fraction was determined by density method. As shown in Fig. 7(a), oxygen permeability rapidly decreased with the amount of crystalline fraction, indicating that the β crystalline form, as in the case of most polymers, was most likely impermeable for small gas molecules like oxygen. If the permeation process occurs in the amorphous phase only and crystals represent impermeable and insoluble entities, the solubility coefficient, which represents an additive function of the solubilities of crystalline and amorphous phases, must

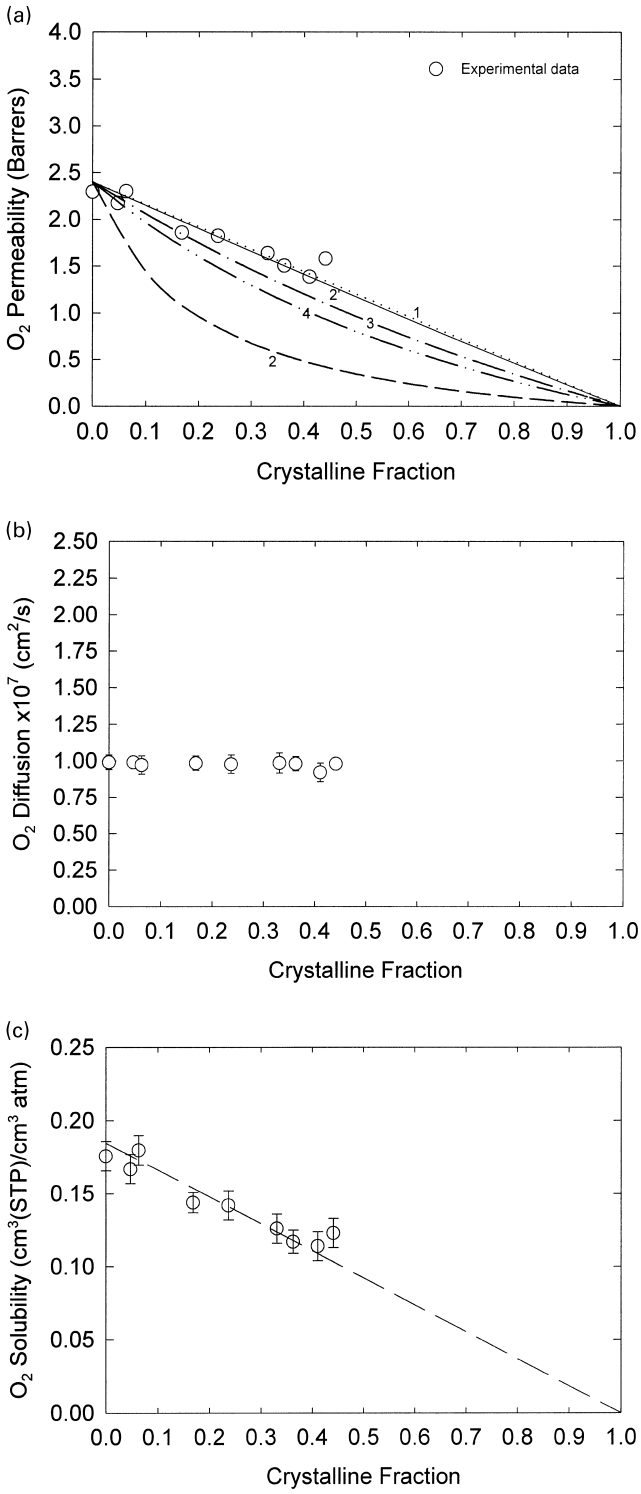

Fig. 7. Effect of crystallinity on oxygen gas permeability (a); diffusion (b); and solubility (c) for melt-crystallized s-PS containing β crystalline form.

decrease linearly with crystallinity due to insolubility of the crystalline phase according to $S = S_a(1 - \phi_c)$ where S_a is the solubility of the amorphous phase and ϕ_c is the amount crystalline phase. Fig. 7(c) shows the solubility coefficient versus the amount of crystalline fraction. Within

the experimental scatter, the solubility indeed decreased linearly with the amount of crystalline fraction. Assuming the filler effect to be the major one, it is feasible to correlate the decrease in permeability with morphological features of the crystalline phase. Although permeability of the complex hierarchical structure of the crystalline phase is difficult to model, some simple predictions based on simple filler shape and filler orientation are useful to understand the efficiency of given crystalline structure in obstructing gas permeation. Fig. 7(a) includes the experimental data of oxygen permeability versus crystalline fraction and several simple theoretical predictions of permeability versus the filler volume fraction, ϕ_c for (1) sheets (laminates) or long rods oriented perpendicular to the membrane surface, $P = P_a(1 - \phi_c)$; (2) flakes with aspect ratio ten oriented parallel ($\alpha = 10$) and ($2'$) perpendicular ($\alpha = 0.1$) to the membrane surface, $P = P_a 2(1 - \phi_c)/(2 + \alpha\phi_c)$; (3) impermeable spheres $P = P_a 2(1 - \phi_c)/(2 + \phi_c)$; (4) long rods oriented parallel to the membrane surface $P = P_a(1 - \phi_c)/(1 + \phi_c)$ [18]. Surprisingly, we found that oxygen permeation data for s-PS containing the β form were in a good agreement with the prediction (1) or ($2'$). Hence, the crystallites of the β form produced a very small effect in obstructing the gas permeation. The diffusion data (Fig. 7(b)) also confirmed the low diffusion impedance of the β crystallites. Within experimental scatter, diffusion coefficient did not change with crystallinity suggesting that the crystallites of the β crystalline form had a very small effect on increasing of tortuosity of the diffusion path. This behavior is unusual. At this point we have no morphological or other evidences suggesting why the β crystalline form produced a little effect in obstructing of gas diffusion. Getting these evidences is the scope of our current study.

3.3.2. Analysis of the α crystalline form

Fig. 8(a)–(c) shows oxygen permeability, diffusion and solubility, respectively, versus density crystallinity for samples isothermally crystallized at 260 °C, containing only the limiting ordered modification (α'') of the α crystalline form. The figure also shows the transport data for the sample, which was slowly cooled in the press after compression molding at 280 °C. This sample also contained the α crystalline form. Compared to the β crystalline form, the α crystalline form showed very different gas transport behavior. The permeability and diffusion coefficients increased with the crystallinity (Fig. 8(a) and (b)). However, the solubility decreased down to zero virtually linearly with the crystallinity as in the case with impermeable β phase (Fig. 8(c)). The increase in permeability and diffusion coefficient with crystallinity confirmed that low-density α crystalline form is indeed permeable for small gas molecules like oxygen. The solubility data, however, seemed to disagree with the fact that the α crystalline form is gas permeable. This apparent discrepancy can be resolved if it is assumed that the equilibrium concentration of the dissolved oxygen in the amorphous phase is simply much higher than that in the α crystalline phase. It is widely accepted that the mechanism of gas solubility in glassy amorphous polymers primarily involves the gas molecules filling the excess of free volume, molecular size cavities frozen in the structure of polymer after vitrification [19].

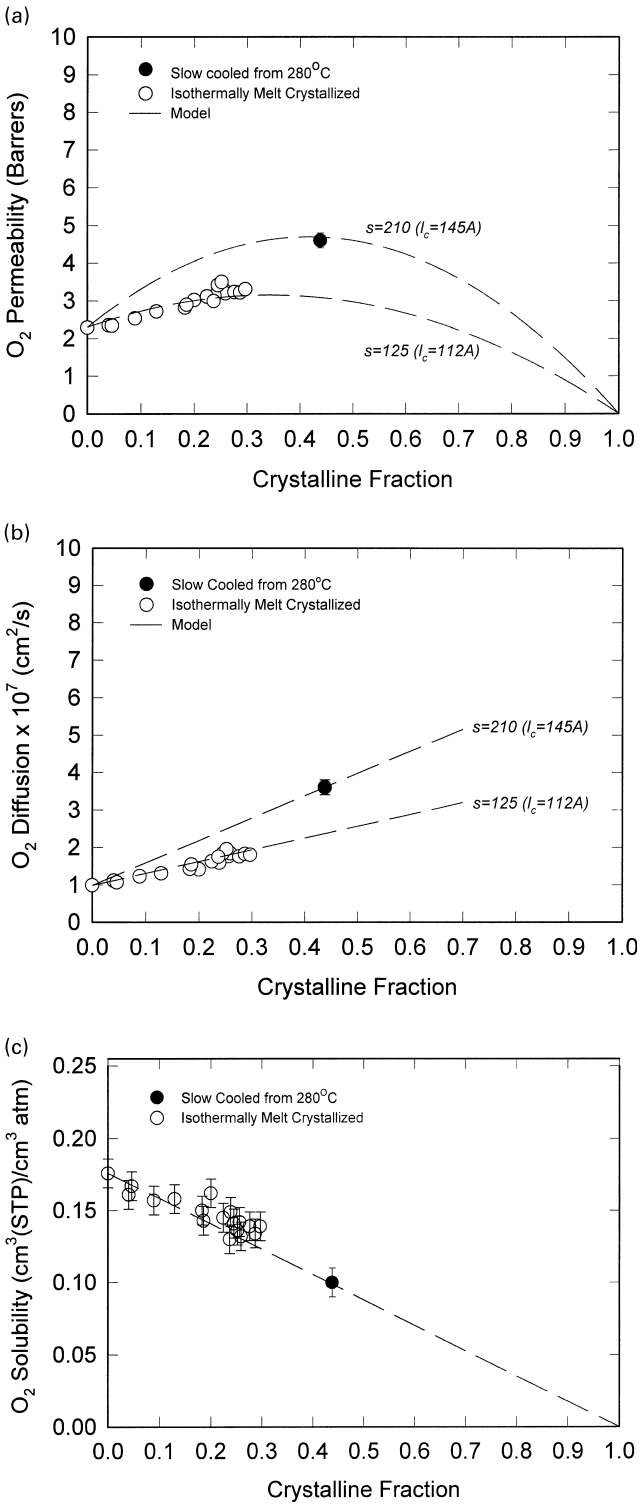

Fig. 8. Effect of crystallinity on oxygen gas permeability (a); diffusion (b); and solubility (c) for melt-crystallized s-PS containing α'' crystalline form.

These cavities act as 'adsorption sites' for gas molecules. Sorption of molecules in the excess of free volume requires considerably less energy than opening a new hole to accommodate a gas molecule in the dense hole-free environment. Low solubility of oxygen in the porous α crystalline structure however is probably due to very low interaction of oxygen with polymer chains of s-PS. In this case, the minima of potential energy and subsequently the adsorption sites are rather associated with the confined environment of microcavities than with 'open-end' environment of the nanochannels.

The mechanism of gas diffusion in the amorphous glassy polymers is often treated in term of 'rattling–jumping' mechanism [20]. According to this mechanism, small gas molecules rattle for a long period of time inside the cavity before jumping to the neighboring cavity. Computer simulations have shown that positions of low energy in which gas molecules spend most of the time truly exist in the structure of glassy, amorphous polymer, as well as the positions of highest energy and saddle points between these adsorption sites [21]. The fraction of gas molecules, which are in the state of 'jumping' is evidently much smaller compared to that existing in the state of 'rattling'. Some of these jumping gas molecules may also hop directly from the microcavities to the channels of the α crystalline structure when the microcavities are located in the close proximity to the crystalline surface. Gas molecules are probably spending a very short time in the 'inconvenient' interior of the channels compared to that which they spend rattling in the cavities. Leaving the channels gas molecules may jump back to the previous cavity or jump to the cavity located on the opposite side of the crystal. Therefore, the porous α crystalline structure serves the role of transmitting media in semicrystalline s-PS making a negligible contribution to the overall gas sorption but significantly accelerating diffusion.

The channels in the α crystals must be oriented parallel to the direction of polymer chains and subsequently, perpendicular to the fold surface of lamella. In this case, the length of the channels must be equal to the lamella thickness. The lamellas in s-PS can be 100–200 Å thick [5]. Presumably, this thickness defines the diffusion length associated with the traveling of gas molecules in the channels. For comparison, the characteristic length of the diffusion jump, which gas molecule similar to oxygen or carbon dioxide makes between the two neighboring cavities in the glassy amorphous polymer, is about 10 Å [22,23]. Therefore, longer jumps in the channels may significantly reduce the overall time gas molecules spend in the polymer during their random walk from one side of the polymer membrane to another side. This should lead to the increase of bulk average diffusion coefficient.

A simple diffusion model, which may describe the main features of gas permeation behavior in semicrystalline s-PS, can be based on a picture, which has an amorphous matrix containing randomly-oriented crystalline lamellas, each having unconnected straight channels aligned perpendicular to the lamellar fold surface. The channel length is equal to the lamellar thickness. We assume very high mobility of gas molecules in the channels in comparison to that in the glassy state. We also assume that sorption of inert gas molecules predominantly occurs in the cavities of the glassy amorphous phase of the polymer. After rattling in a particular cavity, a molecule jumps to another cavity directly or, if the original cavity is located in the close proximity to a crystal channel, jumps to another cavity through the channel. The characteristic time between consecutive jumps for given penetrant sized in either of these two cases is constant, determined by the relaxation properties of the glassy state [22].

The diffusion process then is considered as a random walk, which contains two kinds of uncorrelated jumps with different lengths. Allowing the molecule to travel over a long period of time τ, the number of steps in this random walk N, can be calculated as $N = \tau/\tau_j$, where τ_j is a characteristic time between two jumps. The mean square distance $\langle R^2 \rangle$, covered by a random walk of $N = N_a + N_c$ steps, in which $N_a$is the number of jumps between two cavities directly, and N_c is the number of jumps between two cavities through a channel is:

$$\langle R^2 \rangle = N_a \left\langle l_a^2 \right\rangle + N_c \left\langle l_c^2 \right\rangle, \tag{2}$$

where $\langle l_a^2 \rangle^{1/2}$ is the root mean square distance (jump length) between two cavities in the pure amorphous phase, and $\langle l_c^2 \rangle^{1/2}$ is the root mean square length of the channel equal to the lamella thickness. The same mean square distance $\langle R^2 \rangle$ must also result from an equivalent random walk containing N equal steps, with mean square average step length $\langle l^2 \rangle$ such that

$$\langle l^2 \rangle = \frac{N_a}{N} \left\langle l_a^2 \right\rangle + \frac{N_c}{N} \left\langle l_c^2 \right\rangle \tag{3}$$

The corresponding average diffusion coefficient is given by:

$$\langle D \rangle = \langle R^2 \rangle / 6\tau = N \langle l^2 \rangle / 6\tau \tag{4}$$

Considering a random walk in the pure amorphous polymer over the same time τ, the average diffusion coefficient in the amorphous phase can be expressed as:

$$\langle D_a \rangle = N \left\langle l_a^2 \right\rangle / 6\tau \tag{5}$$

Combining Eqs. (4) and (5), the diffusion coefficient $\langle D \rangle$ in the two-phase model can be expressed in terms of the diffusion coefficient in the pure amorphous phase, $\langle D_a \rangle$, as follows:

$$\langle D \rangle = \langle D_a \rangle \frac{\langle l^2 \rangle}{\left\langle l_a^2 \right\rangle} \tag{6}$$

In expression (3) for $\langle l^2 \rangle$, N_a/N is also the probability, p_a, that the next random step will happen directly between two cavities, which is proportional to the volume fraction of amorphous phase, $p_a = 1 - \phi_c$. In turn, N_c/N is the

probability, p_c, that the next random step will take place between two cavities through the channel, which is proportional to the product of three fractions: the volume fraction of crystalline phase, ϕ_c, the 'target ratio', $\sigma = A_o/A_c$ (A_o is the total channel orifice area and A_c is the total fold surface area of lamella), and the orientation factor ψ. Presumably, for randomly oriented crystallites, $\psi = 1/3$, which assumes favorable orientation of lamellar fold surface toward the direction of the jumping molecule. Thus, combining Eqs. (3) and (6), the bulk average diffusion coefficient $\langle D \rangle$ is given by:

$$\langle D \rangle = \langle D_a \rangle \left[1 + \phi_c \left(\psi\sigma \frac{\left\langle l_c^2 \right\rangle}{\langle l_a^2 \rangle} - 1 \right) \right] \tag{7}$$

In Eq. (7), the ratio $s = \langle l_c^2 \rangle / \langle l_a^2 \rangle$ is the only fitting parameter. D_a and ϕ_c are experimentally measurable quantities, $\psi \equiv 1/3$, and σ can be estimated from the crystal structure taking into account the van der Waals diameters for carbon and hydrogen atoms. In particular, for α crystalline s-PS, we estimate the target ratio $\sigma \approx 0.1$.

Undoubtedly, the proposed simplified model represents only an early attempt to describe the diffusion behavior in very interesting media consisting of porous crystals containing channels and amorphous matrix. In reality, in channel, diffusion may occur through a combination of very frequent but shorter jumps rather than through one, about 100 Å long jump, since it should be some local energy minima in the interior of the channels. However, the detailed mechanism of diffusion in this case can be elucidated only using careful molecular modeling.

The presented model predicts a linear dependence of $\langle D \rangle$ versus crystalline fraction ϕ_c. The slope of the linear dependence $\langle D \rangle = f(\phi_c)$ in the model is then entirely defined by the lamellar thickness for given crystalline and amorphous structure. The applicability of the model becomes questionable when $\phi_c \sim 1$ due to the assumption that diffusion jumps always occur between cavities residing in the amorphous phase. Hence, for the model to work, a reservoir of cavities and consequently, substantial amount of the amorphous phase must be present for diffusion to go on.

Fig. 8(b) shows the diffusion behavior predicted from Eq. (7) for two different values of parameter $s = \langle l_c^2 \rangle / \langle l_a^2 \rangle$. We found a good agreement between the model and experimental data. The best fit (dashed line) of the model to the diffusion data for isothermally melt crystallized at 260 °C samples was obtained for parameter $s = 125$. From $s = 125$, the lamella thickness for samples melt-crystallized at 260 °C was estimated assuming $\langle l_a^2 \rangle^{1/2} \approx 10$ Å. The estimated lamella thickness in this case $\langle l_c^2 \rangle^{1/2} \approx 112$ Å. This value of the lamella thickness is in general agreement with the experimental observations of the lamellar thickness in semicrystalline s-PS [5]. For slowly cooled in the press samples, the best fit was obtained at $s = 210$. This corresponded to the lamella thickness $\langle l_c^2 \rangle^{1/2} \approx 145$ Å. Thicker lamellas for samples slowly cooled in the press were expected, because this crystallization conditions most likely are associated with effectively smaller melt undercooling compared with that upon melt-crystallization at 260 °C. Smaller undercooling presumably led to the increase in average lamella thickness. Therefore, gas diffusion in semicrystalline s-PS containing porous α crystals is not only controlled by the amount of amorphous and crystalline phases, but it is also determined by the crystalline morphology (lamella thickness).

The proposed diffusion model can be further expanded to consider the dependence of permeability versus crystalline fraction. Combining Eq. (7) with the condition that equilibrium sorption takes place in the amorphous phase only, hence $S = S_a(1 - \phi_c)$, with $P = DS$, $P(\phi_c)$ can be expressed as follows:

$$P(\phi_c) = P_a \left[-(\psi\sigma s - 1)\phi_c^2 + (\psi\sigma s - 2)\phi_c + 1 \right] \tag{8}$$

According to Eq. (8), the dependence of $P(\phi_c)$ on ϕ_c is parabolic. When $\psi\sigma s > 2$, the permeability increases monotonically from $P = P_a$ at $\phi_c = 0$, to

$$P_{max} = P_a \left[\frac{(\psi\sigma s)^2}{4(\psi\sigma s - 1)} \right] \quad \text{at} \quad \phi_c = \frac{(\psi\sigma s - 2)}{2(\psi\sigma s - 1)},$$

(diffusion dominating regime), and then decreases monotonically from $P = P_{max}$ to $P = 0$ at $\phi_c = 1$, (solubility dominating regime). The maximum permeability, depending on the lamella thickness, could be found between $0 < \phi_c < 0.5$. It is interesting to note that $\phi_c = 0.5$ corresponds to about the maximum crystallinity, which could be developed in thermally crystallized s-PS. Fig. 8(a) shows the plot of oxygen permeability coefficient versus crystalline fraction (experimental points) and two dependencies $P(\phi_c)$ calculated from Eq. (8) using different values of the parameter s. As expected, for s-PS melt crystallized isothermally at 260 °C, the best agreement between the experimental data and the calculations was obtained for $s = 125$ and for sample slowly cooled in the press $s = 210$. Permeability in semicrystalline s-PS containing α crystalline form, as in the case of diffusion, is not only controlled by the amount of crystallinity but also significantly depends on the thickness of crystalline lamellas.

Fig. 9(a)–(c) shows the plot of carbon dioxide permeability, diffusion and solubility versus crystalline fraction for s-PS melt crystallized at 260 °C containing α'' crystalline phase. Quantitatively, the corresponding trends of carbon dioxide permeability, diffusion and solubility versus crystallinity were similar to those we observed for oxygen. Carbon dioxide solubility of the α crystalline phase was also much smaller than that of the amorphous phase. Carbon dioxide diffusion and permeability for semicrystalline s-PS increased with crystallinity. Diffusion versus crystallinity showed a linear trend. It was interesting to apply the diffusion model for carbon dioxide data in order to find out whether the best fit of the diffusion model would result in

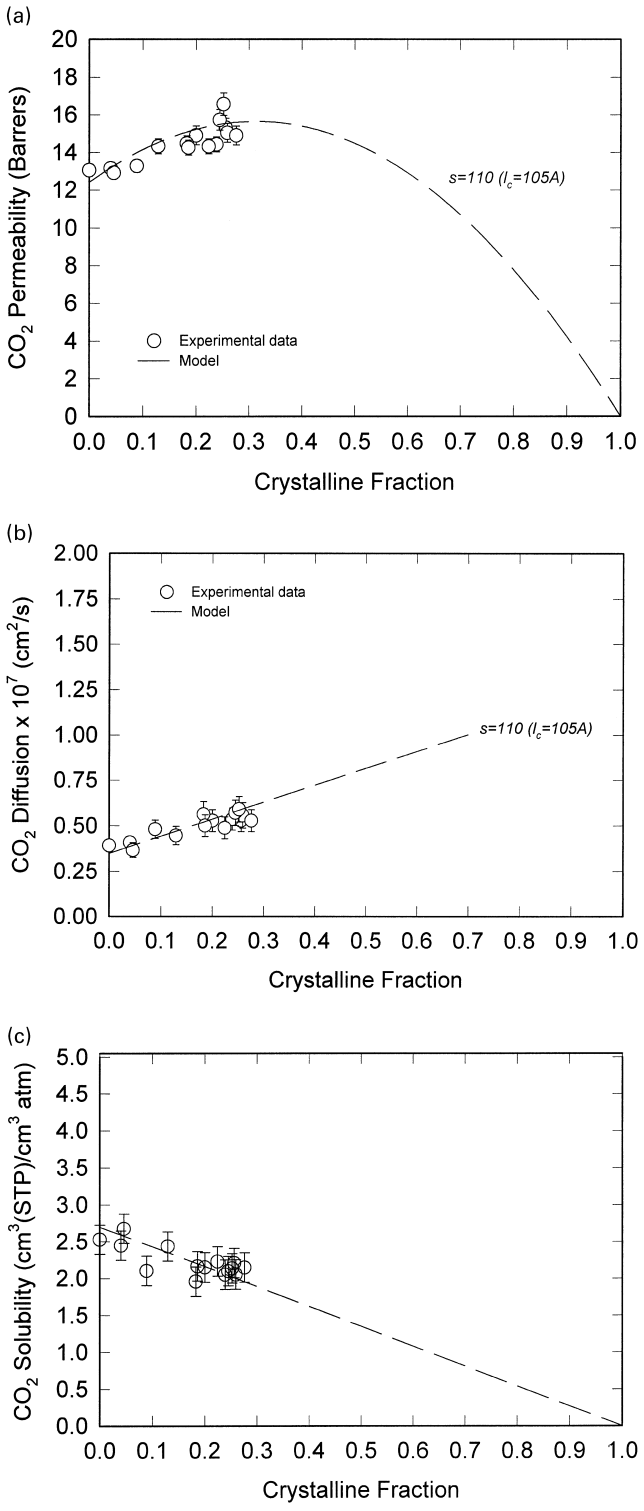

Fig. 9. Effect of crystallinity on carbon dioxide gas permeability (a); diffusion (b); and solubility (c) for melt-crystallized s-PS containing α'' crystalline form.

similar prediction of lamella thickness as in the case of oxygen using the same series of semicrystalline s-PS samples. The best fit of the model to carbon dioxide data was obtained for parameter $s = 110$. Assuming the diffusion jump length for oxygen and carbon dioxide in glassy s-PS to be the same, which probably is a reasonable assumption considering very similar kinetic diameter of these two gas molecules, the lamella thickness $\langle l_c^2 \rangle^{1/2} \approx 105$ Å was calculated. One can see that the lamella thickness predicted from carbon dioxide data, 105 Å, is indeed very close to the lamella thickness, 112 Å, predicted from oxygen data using the same series of semicrysalline s-PS samples.

Fig. 10(a)–(c) shows oxygen permeability, diffusion and solubility for cold-crystallized s-PS containing limiting disordered modification, α', plotted as a function of density crystallinity. The solubility behavior of this crystalline form versus crystallinity (Fig. 10(c)) suggested that it also was much smaller than the solubility of the amorphous phase, as in the case of isothermally melt-crystallized s-PS containing the α'' form. Also, as in the case of s-PS containing the α'' crystals, the diffusion and permeability of semicrystalline s-PS containing the α' crystalline form increased with crystallinity. However, cold-crystallized s-PS containing the α' crystalline form exhibited non-linear dependence of diffusion coefficient versus crystallinity (Fig. 10(b)), which was in contrast with the linear trend of diffusion coefficient versus crystallinity shown by melt-crystallized s-PS (Fig. 8(b)). This behavior can be understood by taking into account that in this work, progressively higher cold-crystallization temperatures were used to develop larger fractions of the α' crystalline phase. Higher cold crystallization temperatures not only produced higher crystallinity but also presumably led to thicker crystalline lamellas. As it was previously discussed, in addition to the degree of crystallinity, the lamella thickness is an important parameter determining the diffusion and permeability in semicrystalline s-PS containing porous crystals. Fig. 9(b) contains several linear predictions $D(\phi_c)$ based on Eq. (7) for different values of parameter s and subsequently, different values of the lamella thickness. One can see from this picture that non-linear trend of the diffusion versus crystallinity, in fact, may represent a collection of small portions of multiple linear trends $D(\phi_c)$ with different slopes resulted from crystals with different lamella thickness formed at different cold-crystallization temperatures. Fig. 10(a) shows several predictions of permeability versus crystallinity based on Eq. (8) using the same values of the parameter s, which was used for diffusion. As in the case of diffusion, the permeability versus crystallinity dependence for cold-crystallized s-PS can also be understood assuming that it consists of a collection of small portions of multiple parabolas characterized by progressively larger values of the parameter s and subsequently larger values of the lamella thickness formed at higher cold-crystallization temperatures.

It was interesting to compare the gas transport properties of pure α'' and α' modifications of the α crystalline form grown at the same crystallization temperature. The temperature 260 °C was used in the case of isothermal melt-crystallization and in the case of cold-crystallization. Despite the fact that s-PS cold crystallized at 260 °C

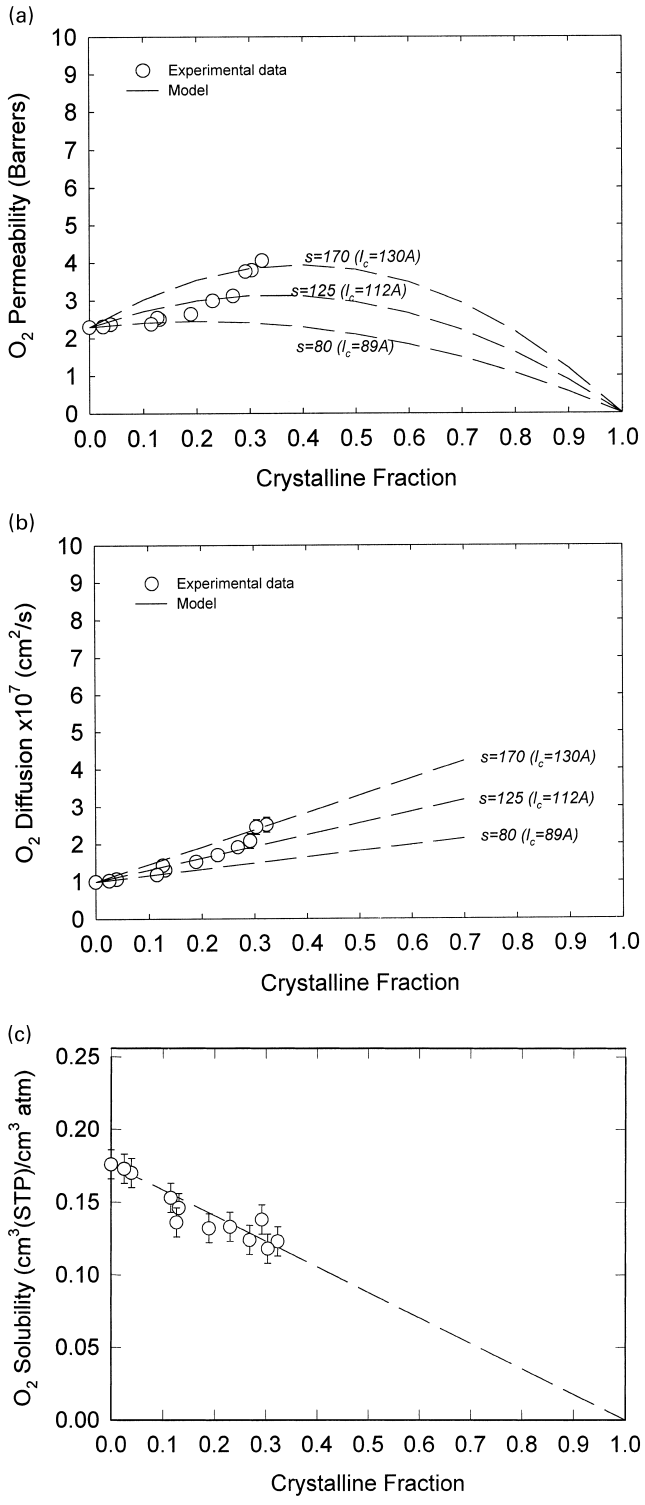

Fig. 10. Effect of crystallinity on oxygen gas permeability (a); diffusion (b); and solubility (c) for cold-crystallized s-PS containing α' crystalline form.

exhibited diffusion and permeability slightly larger than those shown by s-PS melt crystallized at 260 °C (the samples contained similar crystallinities), in general, it still can be concluded that gas transport properties of both limiting ordered (α'') and limiting disordered (α') modifications are similar if they are formed at the same crystallization temperature.

3.4. Sub-T_g relaxation behavior

Sub-T_g relaxation (small scale molecular motions) is typically associated with the amorphous state of polymer and considered to be an important factor determining gas transport in glassy polymers. Inhibiting sub-T_g motions may result in the decrease in diffusion coefficient while disencumbering of sub-T_g relaxation, in turn, may lead to its increase. The crystalline structure of polymers is usually too dense to permit even very small molecular motions; however, low density crystalline structure of the α and β crystalline forms of s-PS raises an interesting question whether small scale molecular motions could also take place in the case of crystalline structure. Fig. 11 shows DMTA traces (tan δ) for atactic polystyrene, amorphous s-PS, melt-crystallized s-PS containing 10, 23 and 40% of the α'' crystalline phase, cold crystallized at 260 °C s-PS containing 32% of the α' crystalline phase, melt-crystallized s-PS containing 30% of the β crystalline phase shown in the temperature range −140 to 50 °C.

Atactic PS was extensively studied in the past [24,25]. Three mechanical relaxation processes T_g were typically reported at about 1 Hz frequency: β relaxation at about 27 °C ($\Delta H^{\neq} \approx 140$ kJ/mol), γ relaxation at about −120 °C ($\Delta H^{\neq} \approx 40$ kJ/mol), and δ relaxation at about −238 °C ($\Delta H^{\neq} \approx 10$ kJ/mol). The δ peak was attributed to oscillation or procession of the phenyl group coupled with wagging motion of the backbone unit attached to the ring. Some researchers associated the γ process with motion of chain ends and some with restricted phenyl group rotation. The molecular origin of the β peak, as in the case of the γ

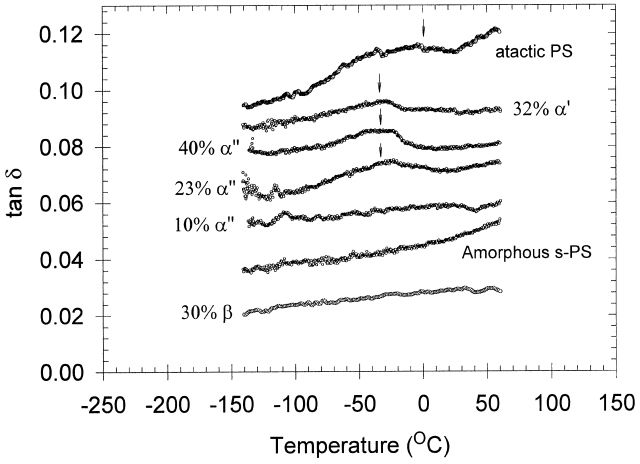

Fig. 11. tan δ at 1 Hz as a function of temperature for amorphous a-PS and s-PS, melt-crystallized s-PS containing 30% of the β crystalline form, melt-crystallized s-PS containing 10, 23 and 40% of the α'' crystalline form, and cold-crystallized containing 32% of the α' crystalline form. Curves are shifted vertically.

relaxation, is also not very clear yet. Some researchers related this relaxation to the rotation of phenyl rings coupled with the backbone motion. The relatively high activation enthalpy for the β relaxation was attributed to the 'matrix effect'. It seems reasonable to assume that the backbone chain in the immediate vicinity of the phenyl ring could also be involved into the relaxation process, so that it would be a composite effect. Some researchers also think that the β peak in a-PS is due to a twisting of the main chains.

In the case of a-PS, we clearly observed the β relaxation peak with an approximate maximum at 10–30 °C. It is very broad, starts at approximately −100 °C and overlaps at high temperatures with the glass transition. We were not able to resolve the γ relaxation peak, and the δ peak was presumably located at temperatures too low to be measured in our experiments. The lowest temperature we were able to begin the measurements was −140 °C. Amorphous s-PS, in contrast to a-PS, showed no sub-T_g relaxation peaks in the range −140 to +50 °C. Even well pronounced in the case of a-PS, the β relaxation peak was absent in amorphous s-PS. It is interesting to note that the β relaxation peak also does not appear in the case of isotactic polystyrene [24]. Therefore, only atactic form of polystyrene demonstrates the β relaxation peak while this transition is apparently absent in the case of stereoregular forms.

Semicrystalline s-PS, containing the β crystalline structure, showed no sub-T_g relaxation, as in the case of amorphous s-PS. In contrast, we found that semicrystalline s-PS polystyrene containing the α crystalline form showed a well-pronounced relaxation peak with a maximum located at about −35 °C. This relaxation peak existed in the case of melt-crystallized s-PS containing α'' modification of the α form and in the case of cold-crystallized samples containing the α' modification of the α form. The magnitude of this relaxation transition increased with crystallinity. Therefore, this new relaxation was attributed to the low-density crystalline structure of the α crystalline form. At this point, we have no direct evidences of what kind of molecular motion is responsible for this relaxation process. One possibility is that this motion could be associated with rotation of the individual phenyl rings or may even include the cooperative motion of the phenyl rings. Any motion associated with the backbone, most likely, is absent in the case of crystalline structure. The apparent next step of this study should be testing the gas permeation behavior of s-PS containing the porous α crystalline form below the temperature of this new relaxation. If this relaxation process is indeed coupled with the gas transport properties of this crystalline form, a severe reduction of bulk average diffusion coefficient is expected. Gas transport measurements of semicrystalline s-PS at different temperatures including sub-ambient are currently ongoing in our lab.

4. Conclusions

Two thermally induced crystalline forms of s-PS exhibited different gas transport behavior. The β crystalline form seemed to be impermeable for transport of oxygen and carbon dioxide. The α crystalline form was found to be highly permeable for transport of oxygen and carbon dioxide. We found gas transport properties of the limiting ordered, α'', and limiting disordered modification, α', of the α form to be similar when prepared at the same crystallization temperature. High gas permeability of the α crystals was associated with porous crystalline structure of this form containing nanochannels oriented parallel to the polymer chain direction. An aperture of these nanochannels, about 4–5 Å wide, allows for the transport of small gas molecules such as oxygen and carbon dioxide to take place in the interior of this unusual crystalline structure. Despite the porous structure, α crystalline form showed very low oxygen and carbon dioxide solubility in comparison with that in the amorphous phase. Thus, the porous α crystalline structure serves the role of transmitting media in semicrystalline s-PS, making a negligible contribution to the overall gas sorption but significantly accelerating the diffusion process by passing gas molecules through the crystalline structure.

The diffusion model, which considered a random walk of gas molecules jumping between the cavities of the amorphous phase either directly or through the longer channels in the crystals, was proposed. The model explained the characteristic features of the gas permeation behavior for chemically 'inert' small gas molecules in the permeation medium consisting of glassy amorphous polymer with dispersed porous crystalline phase containing the nanochannels. The model predicted the linear dependence of gas diffusion versus crystallinity for crystals with same lamellar thickness. The slope of this dependence is defined by the lamellar thickness. The diffusion model was extended toward the permeation and predicted the parabolic dependence of permeability with crystallinity with two regimes of permeation, depending on the amount of crystalline phase, diffusion dominating regime at low crystallinity and solubility dominating regime at high crystallinity. A good agreement of the model with the experimental data was observed. The model explained the non-linear dependence of diffusion coefficient versus crystallinity for s-PS cold crystallized at various temperatures.

Semicrystalline s-PS containing porous α crystalline form exhibited unknown mechanical relaxation peak with a maximum at about −35 °C. New relaxation process was attributed to the low-density crystalline structure of the α form.

Acknowledgements

Acknowledgment is made to the donors of The Petroleum Research Fund, administrated by the ACS, for support of this research. The research was also generously supported by the National Science Foundation through Grant

DMR-9986467 and Grant DMR-9975774 (Polymer Program, Division of Material Research). Authors also thank the Dow Chemical Company for providing polymers for this research. Support from Modern Controls, Inc. for development of a facility for gas-transport studies at Case Western Reserve University is gratefully acknowledged.

References

[1] Guerra G, Vitagliano VM, De Rosa C, Petraccone V, Corradini P. Macromolecules 1990;23:1539.
[2] Chatani Y, Fujii Y, Shimane Y, Ijitsu T. Polym Prep Jpn (Engl Edn) 1988;37:E428.
[3] Sun Z, Morgan RJ, Lewis DN. Polymer 1992;33:661.
[4] De Rosa C, Guerra G, Petraccone V, Corradini P. Polym J 1991;23:1435.
[5] Greis O, Xu Y, Asano T, Petermann J. Polymer 1989;30:590.
[6] De Rosa C. Macromolecules 1996;29:8460.
[7] Cartier L, Okihara T, Lotz B. Macromolecules 1998;31:3303.
[8] De Candia F, Ruvolo Filho A, Vittoria V. Colloid Polym Sci 1991;269:650.
[9] Auriemma F, Petraccone V, Dal Poggetto F, De Rosa C, Guerra G, Manfredi C, Corradini P. Macromolecules 1993;26:3772.
[10] Hodge K, Prodpran T, Shenogina NB, Nazarenko S. J Polym Sci: Part B, Polym Phys 2001;15:2519.
[11] Puleo AC, Paul DR. Polymer 1989;30:1357.
[12] Sekelik DJ, Stepanov EV, Nazarenko S, Schiraldi D, Hiltner A, Baer E. J Polym Sci: Part B, Polym Phys 1999;37:847.
[13] De Rosa C, Rapacciuolo M, Petraccone V, Corradini P. Polymer 1992;33:1423.
[14] Chatani Y, Shimane Y, Ijitsu T, Yukinari T. Polymer 1993;34:1625.
[15] Pasztor Jr AJ, Landes BG, Karjala P. J Thermochim Acta 1991;177:187.
[16] Samulski ET. In: Mark JE, editor. Physical properties of polymers. Washington, DC: ACS, 1993. p. 201.
[17] Alger MM, Stanley TJ. J Appl Polym Sci 1988;36:1501.
[18] Petropoulos JH. J Polym Sci, Polym Phys Ed 1985;23:1309.
[19] Koros WJ, Chern RT. In: Rousseau RW, editor. Handbook of separation process technology. New York: Wiley, 1987. p. 862.
[20] Petropoulos JH. In: Paul DR, Yampol'skii YP, editors. Polymer gas separation membranes. Ann Arbor: CRC Press, 1994. p. 17.
[21] Theodorou DN. In: Neogi P, editor. Diffusion in polymers. New York: Marcel Dekker, 1996. p. 67.
[22] Haward RN, Young RJ. The physics of glassy polymers. London: Chapman & Hall, 1997. p. 76.
[23] Stannett V. In: Crank J, Park JS, editors. Diffusion in polymers. New York: Academic Press, 1968. p. 42.
[24] Roberts GE, White EFT. In: Haward RN, editor. The physics of glassy polymers. New York: Wiley, 1973. p. 153.
[25] Cowie JMG. J Macromol Sci-Phys 1980;B18:569.